Numerical Study of Heat and Mass Transfer of MHD Casson Fluid Flow with Cross-Diffusion and Heat Source Impacts in presence of Radiation

Shilpa[1], *Ruchika Mehta*[1*], *Sushila*[2]*and Renu Sharma*[3]
[1]*Department of Mathematics and Statistics*,
Manipal University Jaipur, Jaipur(Raj.), India
[2]*Department of Physics*,
Vivekananda Global University, Jaipur(Raj.), India
[3]*Department of Physics*,
JECRC University, Jaipur(Raj.), India
[1*]*ruchika.mehta*1981@*gmail.com*

Abstract

The current research analyzes Soret and Dufour effects on magneto hydrodynamic natural convection viscous-elastic radiative Casson fluid flow across a non-linear stretchy sheet. First, the PDEs (partial differential equations) are changed using similarity analysis into non-linear paired ODEs (ordinary differential equations). Then, using the BVP4C technique, ordinary differential equations are numerically solved. Engineering interest of substantial quantities like skin-friction coefficient, Nusselt parameter, and Sherwood parameter debated in the table with multiple significant characteristics. The current study describes that the temperature profile increases with rising thermal radiation and the Dufour effect. A declining Sherwood impression of Soret number is depicts in current study. An increasing radiation impact declines the Nusselt number.In addition, the concentration field enhances due to an increasing Soret effect.

Key words: Non-linear stretchy sheet, Soret and Dufour effects, Casson fluid, Radiation Parameter, BVP4C technique.

1 Introduction

When most organic and commercial fluids, including hemoglobin, printer inks, greasing heavy oils, watercolors, gypsum pastes, fluid cleansers, multigrade oils, ceramic materials, fruit drinks, polymeric materials and others are pressured, they modify their initial fluid properties or viscosity nature. The traditional Newton's law of viscosity is significantly deviated by these non-Newtonian fluids. Many Researchers have explore a variety of non-Newtonian viscous-elastic flow samples through evaluate their unique flow movement in order to estimate these conventional fluids' features of flow, temperature and concentration dispensation in a suitable way.

Thermal radiation is the process through which energy or heat is conveyed by electromagnetic waves. Thermal radiation is important when there is a large temperature difference between the boundary surface and the surrounding fluid. In physics and engineering, radiative impacts are essential. The effects of radiation heat transfer on various flows are critical when performing activities requiring high

temperatures and space technologies. For instance, the effects of radiation are essential for observing heat transfer in the polymer sectors, where heat regulating elements have a mild influence on the quality of the finished product. Relevant are also the effects of radiation on nuclear power plants, aircraft, gas turbines, spacecraft, liquid metal fluids, and solar radiation.A comprehensive examination of mixture convective flow of Casson and Oldroyd-B fluids through a linearly stratified stretchy sheet was reported by Kumam, P.et al. [1]. Additionally Thermal radiation, chemical reactivity, and magnetization are all properties of Casson and Oldroyd-B fluids. The property of slide boundary circumstances and chemical reactive on heat and mass transport via mix convective boundary stratum flow of a non-Newtonian fluid over a non-linear stretchy sheet are studied by Ahemed et al. [2]. Ahmad. et al. [3] studied the free convection slippage flow of fractional viscous fluid by considering the thermal radiation, heat generation, chemical reaction of order first, and Newtonian heating through a porous medium by considering single-wall carbon nanotube (SWCNT).The Casson fluid form is used to explain the performance of non-Newtonian fluids. Basha et al. [4] investigated the MHD convective heat transport viscous-elastic boundary layer of the Casson fluid with Joule and viscous dissipation characteristics under the impact of chemical process and in the presence of Lorentz forces, a non-linear stretched sheet was utilized. Basha et al. [5] developed a 2D numerical form to explore the result of buoyancy forces on magnetized free convective Walters-B fluid flow across a stretched sheet with Soret impact, heat radiative, heat source/sink, and viscous dissipation. The stretchy sheet geometry is used to generate the present physical model. The electromagnetic force on a charged particle, effect on a non-linear structure is analyzed. The work focuses exclusively on contributions to the utilization of non-Newtonian Casson fluid entropy generation across an exponentially stretched sheet. Entropy generation and homogeneous–heterogeneous reactions are explored by Das et al. [6]. Instead of no-slip situation at the boundary, motion and thermal slips are measured. The buoyancy influence on 2D Casson fluid flow and mix convection over a non-linear stretched sheet is detected from Gangadhar et al. [7].

The Soret effect is related to mass flow phenomena caused by heat diffusion, while the Dufour effect is tied to the energy flux generated by the solute difference. The Soret impact is used to cope with gas concentrations with lighter and medium molecular weights. The Soret and Dufour phenomena are used to transfer heat and mass in a variety of industrial and engineering applications, such as multicomponent melts in geosciences, groundwater pollutant migration, solidification of binary alloys, chemical reactors, space cooling, isotope separation, oil reservoirs, and mixtures of gases.An unsteady free convection slip flow of second grade fluid over an infinite heated inclined plate solved with Caputo-Fabrizio fractional derivativeis studied by Haq et al. [8].Hussanan et al. [9] explored the heat transfer from a Casson fluid to a non-linearly expanding sheet using Newtonian heating and the magneto hydrodynamic flow of that fluid. Ibrahim et al. [10] constructed a mathematical model for the investigation of mixed convection on MHD Casson fluid flow through a non-linearly permeable extended sheet with radiative, viscous dispersion, heat source/sink, chemical reaction, and suction. They also used the Buogiorno's type Nano-fluid form, which includes Brownian motion and thermophoresis. The impacts of radiation parameter and chemical reactions on time dependent MHD free convection flow in a porous plate were analyzed by Matta et al. [11].Mehta. et al. [12] discussed magnetohydrodynamics varied convective stagnation point stream with a vertically extended sheet embedded in a permeable material with generation/absorption, radiation impacts, and viscous dissipation. The MHD flow stalling at the point of Casson fluid across a non-linearly extending sheet with viscous dispersion was studied from Medicare et al. [13].The MHD flow and heat transmission of Casson nano particles across a non-linear (temperature variation

throughout) stretchable sheet is studied by Mustafa et al. [14]. Mukhopadhyay, s. [15] explored a boundary layer investigation for non-Newtonian fluid flow and heat transport across a non-linearly stretchy sheet. The motion field is suppressed when the Casson constraint is rised. However, as the Casson parameter is enhanced, the temperature rises. In the existence of a chemical reaction, Naduvinamani et al.[16] explored the heat and mass transport characteristics of a time dependent MHD squeeze flow of Casson fluid between two parallel plates with viscous and Joule dissipation influences. Compress flow is affected by Soret and Dufour impacts, as well as radiation parameter and heat source/sink impacts are explored. Panigrahi et al. [17] assessed the effects of Soret and Dufour on the properties of heat and mass transport in a mixture Powell-Erying fluid boundary layer flow on a non-linear stretch sheet. In the existence of thermal radiation and chemical reaction, Reddy et al.[18] studied the time independent 2D MHD convective boundary layer flow of a Casson fluid over an increasingly slope porous stretchy sheet.

Aside from the flow caused by an unstable or steady extending/shrinking sheet, the influence of the buoyant force caused by the stretching sheets could not be ignored. The importance of thermal radiation with mixed convective boundary layer (BL) flow in geothermal engineering, space technology, and nuclear reactor cooling has increased interest in the topic.Singh et al. [19] investigate thin film flow of a third-grade fluid down a inclined planeusing an effective well organized computational scheme namely homotopy perturbation Elzaki transform method.Singh et al. [20] studied the local fractional linear transport equations (LFLTE) in fractal porous media.Sumalatha and Bandari [21] investigated the impact of radiation impact and heat source/sink on the flow across a non-linearly expanding sheet of Casson fluid. Sreedevi et al. [22] studied the convective heat and mass transport flow of an electrical conducting fluid over a porous vertically stretched sheet under the assorted property of the magnetic parameter, Joule heating, thermal radiation absorption, viscous dissipation, buoyancy forces, Soret, and Dufour. Tak et al. [23] examined the impressions of radiation parameter and magnetic impact on the heat and mass transport features of natural convection around an upright surface embedded in a dripping wet Darcian porous media, taking into account the Soret and Dufour impacts. Ullah et al. [24] explored the impact of slip effects on MHD free convection flow of non-Newtonian fluid across a non-linear stretched sheet wringing wet in porous media with Newtonian heating. Ullah et al. [25] investigated a time dependent mix convection flow of Casson fluid for a non-linear extending sheet with slip and convective boundary circumstances. Furthermore explored are the impacts of thermo-diffusion, diffusion-thermo, viscous dissipation, and heat Source/Sink. The flow and heat transport characteristics of a viscous fluid over a non-linear extending sheet are investigated through studied by Vajravelu, K. [26].

Basha, H. et al. [4] are investigated the Casson fluid flow natural convection viscous-elastic boundary layer in MHD over a non-linear stretched sheet with Joule and viscous dissipation impacts under chemical reaction influence in the presence of Lorentz forces. The current work fills the gap of Basha, H. et al. [4] by involving the Soret and Dufour impacts in existence of radiation parameter, and the numerical result discussed through graphs along with table using MATLAB software.

2 Problem Structure:

The current study examines the movement of 2D; time-independent, laminar, viscous, incompressible boundary layer carrying a MHD Non-Newtonian Casson fluid across a non-linear stretched sheet. Based on the geometry that is taken into consideration, the current physical condition is modeled. On the other hand, Figure 1 gives clear clarification of the measured problems flow configuration completed with

all required criteria. The contemplated flow design is consistent with the $y = 0$ plane and stream are restricted to just $y > 0$. Still, exterior forces are used in combination with axial flow side in which the surface is enhanced and the origin is fixed. In order to clearly give details the problem, the authors also established a rectangular system where the y-direction is taken perpendicular to the stretchy surface and the x-coordinate is measured along the flow direction. Also, B_0 strength is applied to the Y-coordinate, as is seen in Fig. 1. Furthermore; the free flow velocity, thermal, and volume fraction are represented by U_∞, T_∞, and C_∞.

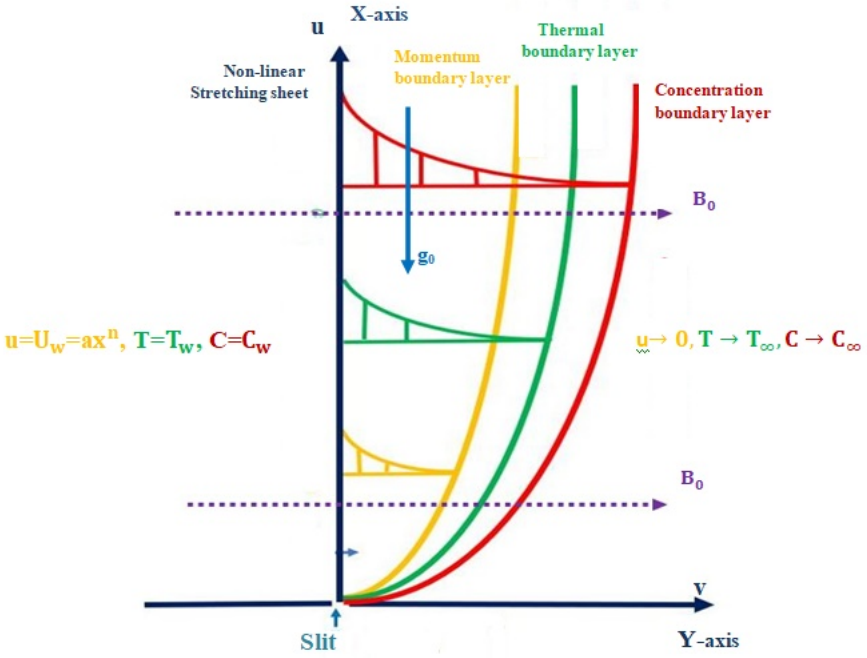

Figure 1: Physical structure and coordinate system of the topic under investigation.

The established equation of a Casson fluid is inscribed by used Ref [4], [7], [9], and [15]

$$\tau_{mn} = \begin{cases} 2(\mu_B + \frac{\tau_y}{\sqrt{2\pi}})e_{mn} & \text{if } \pi > \pi_c \\ 2(\mu_B + \frac{\tau_y}{\sqrt{2\pi}})e_{mn} & \text{if } \pi < \pi_c \ . \end{cases} \tag{1}$$

Where $\pi = e_{mn}e_{mn}$ and e_{mn} is the $(m, n)^{th}$ section of the rate of deformation, π is the multiple of the sections of defacement rate, π_c is critical worth of the multiply founded by the non-Newtonian fluid form, μ_B is the plastic movable viscosity of the non-Newtonian fluid and τ_y is the yield stress of the fluid.

The following criteria define the controlling relations for the proposed study Ref. [4], [17], [18]

$$\frac{\partial u}{\partial x} + \frac{\partial v}{\partial y} = 0, \tag{2}$$

$$u\frac{\partial u}{\partial x}+v\frac{\partial v}{\partial y}=\nu(1+\frac{1}{\beta})\frac{\partial^2 u}{\partial y^2}-\frac{\sigma {B_0}^2 u}{\rho}+g\beta_T(T-T_\infty)+g\beta_C(C-C_\infty), \tag{3}$$

$$u\frac{\partial T}{\partial x}+v\frac{\partial T}{\partial y}=\frac{k}{\rho c_p}\frac{\partial^2 T}{\partial y^2}+\frac{Q_0}{\rho c_p}(T-T_\infty)+\frac{\mu}{\rho c_p}(1+\frac{1}{\beta})(\frac{\partial u}{\partial y})^2+\frac{\sigma {B_0}^2 u^2}{\rho c_p}$$
$$-\frac{1}{\rho c_p}\frac{\partial q_r}{\partial y}+\frac{D_m K_T}{c_s c_p}\frac{\partial^2 C}{\partial y^2}, \tag{4}$$

$$u\frac{\partial C}{\partial x}+v\frac{\partial C}{\partial y}=D_m\frac{\partial^2 C}{\partial y^2}+\frac{D_m K_T}{T_m}\frac{\partial^2 T}{\partial y^2}-k_1(C-C_\infty). \tag{5}$$

Earlier, equations (2) to (5) are in paired form, $\beta=\mu_B\frac{\sqrt{2\pi_C}}{\tau_y}$ is a parameter for the Casson fluid. And motion factors are u and v. and ν denotes kinematic viscosity, β is a number of the shear thinning Casson fluid, σ shows the electro conductivity, B_0 signifies the magneto field strength, ρ symbol for the density, k denotes thermal conductivity, T pointed for temperature, Q_0 characterizes inside heat source (>0)/sink (<0) amount, C is the occurrence of concentration, D_m defines diffusivity, and k_1 shows the chemical reactive parameter, μ symbol for the dynamic viscosity, C_p represents for the specific heat capacity, C_s is the volume fraction susceptibility, g is the gravitational force, β_T and β_C are the coefficients of thermal and mass expansion. Where the non-linear stretchy surface speed is represented by the parameters a ($a>0$) and n. further the terms $\rho-\rho_\infty=-(\beta_T(T-T_\infty)+\beta_C(C-C_\infty))$ is buoyancy effects. Furthermore, the boundary-layer supposition suggests that corporally the conditions on a particular location are directly dependent upon those upstream. From a mathematical standpoint, the behavior of the system was converted from an elliptical to a parabola form, additionally; this change would significantly simplify the mathematical studies of the problem.

The limitations are composed by used Ref. [4]

$$u=u_w=ax^n,\ v=0,\ T=T_w,\ C=C_w,\ \ at\ y=0.$$

$$u\to 0,\qquad T\to T_\infty,\qquad C\to C_\infty,\qquad at\ \ y\to\infty. \tag{6}$$

the Roseland approximation of the radiation heat flow is defined by Ref. [18], [21]

$$q_r=\frac{-4\sigma}{3k^*}\frac{\partial T^4}{\partial y}, \tag{7}$$

Inscribe the T^4 as a linear connection of thermal with Taylor's series extension regarding expansion about T_∞ and deleting greater terms, we get

$$T^4\approx 4{T_\infty}^3 T-{T_\infty}^4. \tag{8}$$

In view of the similarity transformation, we change the dimensional governing equation into non-dimensional equations and similarity transformation are written as

$$u=ax^n f'(\eta),\qquad v=-x^{(n-1)/2}\sqrt{\frac{\nu a(n+1)}{2}}[f(\eta)+\frac{(n-1)}{(n+1)}\eta f'(\eta)], \tag{9a}$$

$$where \quad \eta = y\sqrt{\frac{a(n+1)}{2\nu}}x^{(n-1)/2}, \quad \theta(\eta) = \frac{T-T_\infty}{T_w-T_\infty}, \quad \phi(\eta) = \frac{C-C_\infty}{C_w-C_\infty}. \text{(9b)}$$

With the help of equations (7) to (9b), equations (2) to (6) are diminished to the following regime with rejecting pressure gradient.

$$(1+\frac{1}{\beta})f''' = \frac{2n}{(n+1)}(f')^2 - ff'' + 2Mf' - G_T\theta - G_C\phi = 0, \tag{10}$$

$$((1+Nr))\theta'' + 2QPr\theta + Prf\theta' + (1+\frac{1}{\beta})PrEc(f'') + 2PrMEc(f')^2 + Dupr\phi'' = 0, \tag{11}$$

$$(1+ScSr)\phi'' + Scf\phi' - 2ScKr\phi = 0. \tag{12}$$

With suitable boundary circumstances

$$f(0) = 0, \quad f'(0) = 1, \quad \theta(0) = 1, \quad \phi(0) = 0, \quad at \ \ \eta = 0. \tag{13a}$$

$$f'(\infty) \to 0, \quad \theta(\infty) \to 0, \quad \phi(\infty) \to 0, \quad at \ \ \eta \to \infty. \tag{13b}$$

Where,M shows the magnetic parameter or Hartman number $M = \frac{\sigma B^2(0)}{\rho a(n+1)x^{n-1}}$, G_T and G_C represent the local Temperature Grashof number $G_T = \frac{g\beta_T(T_w-T_\infty)}{a^2x^{2n-1}\frac{(n+1)}{2}}$ and local Concentration Grashof number $G_C = \frac{g\beta_C(C_w-C_\infty)}{a^2x^{2n-1}\frac{(n+1)}{2}}$ respectively, Pr shows the Prandtl number $Pr = \frac{\nu\rho C_p k}{}$, Nr denotes the Radiation parameter $Nr = \frac{16\sigma {T_\infty}^3}{3kk^*}$, Ec denotes the Eckert number $Ec = \frac{a^2x^{2n}}{c_p(T_w-T_\infty)}$, Du specifies the Dufour number $Du = \frac{D_mK_T(C_w-C_\infty)}{c_sc_p\nu(T_w-T_\infty)}$, Sc denotes the Schmidt number $Sc = \frac{\nu}{D_m}$, Sr represents the Soret number $Sr = \frac{D_mK_T(C_w-C_\infty)}{T_m\nu(T_w-T_\infty)}$, β denotes the non-Newtonian Casson parameter$\beta = \mu_B\frac{\sqrt{2\pi_C}}{\tau_y}$, Kr shows that the chemical reaction $Kr = \frac{K_1}{a(n+1)x^{n-1}}$, where K_1 stands for porosity parameter$K_1 = \frac{\nu}{kc}$, and Q denotes the heat sorce sink $Q = \frac{Q_0}{\rho ac_px^{n-1}}$.

Physical Quantities:

Skin Friction Coefficient Cf_x: The physical amount Skin friction Cf_x that getsup due to the viscous stretch in the surroundings of the plate is well-defined as

$$Cf_x = \frac{\tau_w}{\rho u_w^2}, \quad where \ \ \tau_w = (\mu_B + \frac{\tau_y}{\sqrt{2\pi}})(\frac{\partial u}{\partial y})_{y=0}. \tag{14}$$

Heat Transfer Coefficient: The dimensionless Nusselt number(Nu_x) is specified by

$$Nu_x = \frac{xq_w}{k(T_w-T_\infty)}, \quad where \ \ q_w = -k(\frac{\partial T}{\partial y})_{y=0}. \tag{15}$$

Mass Transmission factor: The amount of mass transport is resulting through a Sherwood parameter (Sh_x) which is assumed by

$$Sh_x = \frac{xq_m}{D_m(C_w-C_\infty)}, \quad where \ \ q_m = -D_m(\frac{\partial C}{\partial y})_{y=0}. \tag{16}$$

Here τ_w denotes the shear stress along with the shrinkage wall, q_w signifies heat flux, and q_m is mass transmission quantity at wall.

Therefore, in terms of Equations (9a) to (9b), the following non-dimensional quantities are obtained:

$${Re_x}^{1/2}Cf_x = (\frac{n+1}{2})^{1/2}(1+\frac{1}{\beta})f''(0),$$

local Nusselt

$$Re_x{}^{-1/2}Nu_x = -(\frac{n+1}{2})^{1/2}\theta'(0),$$

local Sherwood

$$Re_x{}^{-1/2}Sh_x = -(\frac{n+1}{2})^{1/2}\phi'(0). \tag{18}$$

Where, $Re_x = \frac{u_w x}{\nu}$ is the local Reynolds number, Cf_x is Skin Friction coefficient, Nu_x is Nusselt number, Sh_x is Sherwood parameter,τ_w indicates the wall shear stress, k signifies the thermo nano-fluid conductivity, q_w shows the surface heat flux, and q_m directs the surface mass flux.

We resolve the reduced equations (10) to (12) with limit conditions (13a) and (13b) via BVP4C method.

3 Results and Discussion:

The current research attempts to provide a fundamental physical understanding and industrial level practical significance of the subject under consideration. The rheological equations (10 to 13b)are solved numerically with the BVP4C with rheological quantities heat source/sink parameter, generative/destructive, chemical reactive parameter, transverse magnetic impact, thermal diffusivity, viscous dissipation, chemical reaction, radiation parameter, Dufour and Soret effect.Such as n,G_c,G_T, β, M, Ec, Pr, Kr,Nr,Sr,Q,Du, and Sc.For existing study, The Fig. of different parameters is designed with the service of MATLAB software and shown in Fig. 2 to Fig.25. Fig. (2-4) presents how the effects of β on flow sensibility, temperature, and mass transport characteristics. Additionally, the impacts of β on the dominant motion profile are also seen in Figure 2. The flow velocity in the domain of the solution under consideration is significantly reduced by the increasing under the impression of the magnetic and non-linear stretchy parameters, like shown in Figure 2.Flow velocities are decreased for increasingβ because an enhance in β rises the dynamic viscosity when stresses are present, that significantly increases the resistance to the movement of fluid near the wall. Therefore, flow velocity was decreased.Figure 3 also displays the effect ofβ thermal dispersion. This figure shows that the thermal graph decomposes as β rises. The thermal layer is also seen to be thinning.The temperature profile drops to zero until it is close to the surface.Like this, Figure 4 depicts the effect of the Casson fluid parameter on the mass distribution field.The concentration distribution increases near the stretching surface as β increases. Greater β values result in stronger molecular scale contacts, which increase molecular mobility and, ultimately, enhance the fluid's mass distribution. A thicker concentration boundary layer is subsequently observed.Figure 5 shows that the thermal distribution enlarges at greater values of the Dufour impact Du. this can be decoded that rise in the Dufour effect Du, which reason an enhancement in the concentration gradient and a faster rate of mass diffusion. The rate of heat transport associated to the particles rises as an outcome. The thermal profiles improve as a result. Velocity and Temperature decreases with increasing Eckert parameter Ec which is shown in Fig.-6 and 7, respectively. The purpose of Figs. 8 and 9 is to see how local concentration (local concentration Grashof number G_c) affects velocity and concentration. As G_c rises, an enhancement in fluid velocity is seen. As G_c increases, the buoyant force increasingly outweighs the viscous force. As a result, the Grashof number improves fluid flow, raising both the velocity and thickness of the motion barrier layer.Additionally, since the buoyancy force tends to make the concentration gradient higher, the concentration is reduced.

Fig.10-12 shows that the influence of local temperature Grashof number G_T on motion, thermal and volume fraction. For the decrease in the thickness of the boundary layer the motion reduces with rising values of the local temperature Grashof

effect. For increasing the local temperature Grashof parameter, the thermal and volume fraction profiles decrease. This decrease in temperature and concentration profiles is primarily caused by the fact that raising the local temperature uses more energy and causes more heat to flow to the surrounding fluid, which lowers the thermal and volume fraction profiles. Figure 13 shows that the mass distribution degraded at increasing Kr parameters. This decline in Solutal graph is mostly caused by the increased mass distribution that also reduces the concentration distribution. The decreased velocity profile for the increasing Magnetic field M values is depicted in Fig. 14. The resistance grows as the Lorentz forces increase, which causes the velocity distribution close to the surface to flatten. Additionally, for an increasing magnetic impact in the flow field, the factor of the velocity distribution along the axial side decrease to nil at a greater distance from a given point. Consequently, when the magnetic field increased, the velocity field degraded. Figures 15 and 16 explain the impact magnetic parameter M has on thermal and volume fraction flow formulation. The temperature distribution increased for the growing magnetic field M, as seen in Figure 15. Based to the fluid's Joule heating, the temperature field grows as the magnetic field rises since more thermal energy will be liberated into the fluid as an outcome. Even as flexibility stress parameter lowers due to an enhance in the magnetic parameter, the thermal field is augmented in the fluid flow under consideration. Figure 16 also shows how the magnetic field affects the concentration profile. The concentration distribution is seen to react as a decreasing function of magnetic number in this graph.

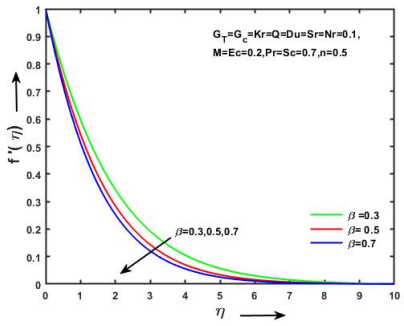

Figure 2: Motion formulation of Casson fluid parameter β.

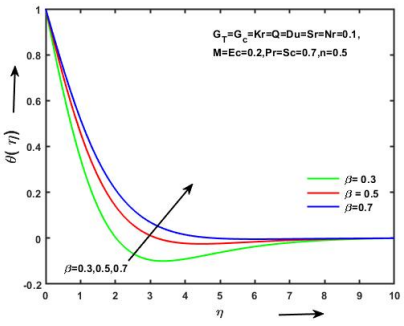

Figure 3: Thermal formulation of Casson fluid parameter β.

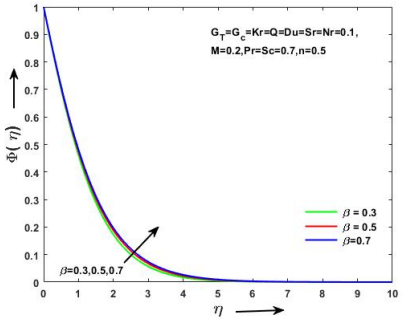

Figure 4: Concentration formulation of Casson parameter β.

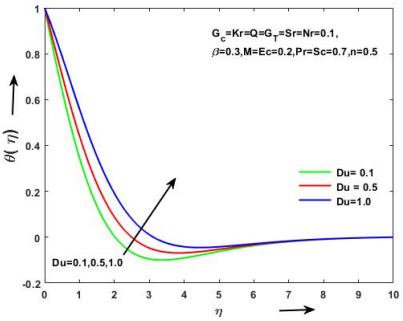

Figure 5: Temperature formulation of Dufour effect Du.

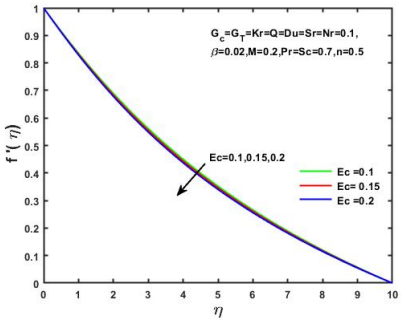

Figure 6: Velocity formulation of Eckert number Ec.

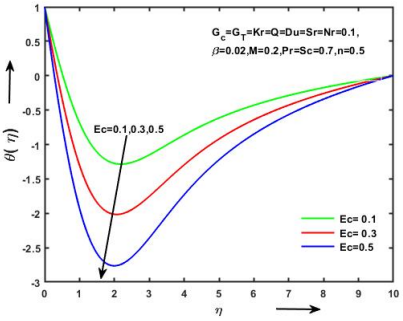

Figure 7: Temperature formulation of Eckert number Ec.

Figures (17–19) show how non-linear stretched parameters affect velocity, temperature, and concentration distribution behavior. Figures 17 illustrate how the expanding stretching variable reduces flow velocity. Additionally, at higher n numbers, this decrease in $f^{'}(\eta)$ is quite small. Since $\frac{2n}{n+1}$ is the coefficient in Equation (10) approaches 2 when $n > 1$, and an outcome the velocity profile is reduced. Additionally, the non-linear parameter n causes the velocity profile to be more disconnected. Furthermore, at a greater distance from the fixed value, the velocity profile monotonically decreased to zero. Figures 18 and 19 show, correspondingly, how the non - linear stretched parameter affects thermal and volume fraction profiles. The thermal and Solutal curves are magnified for the enhancing non - linear parameter n, as shown in Figures 18 and 19. Additionally, at a greater distance from the object, temperature and concentration exponentially decrease to zero. Also, as the non - linear stretched number n increases, the temperature and concentration boundary regions get thicker. As seen in figure.20, temperature is rising as the radiation parameter Nr and the boundary layer thickness it depends on both grow. This is because a rise in the radiation parameter heats the fluid more, which raises the temperature and thickens the layer of thermal boundaries

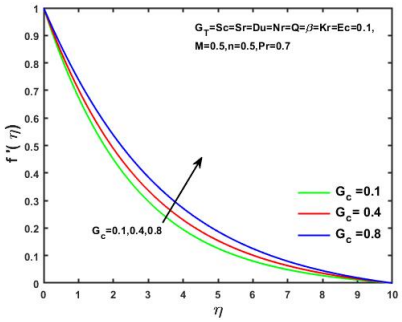

Figure 8: Velocity formulation of concentration Grashof number G_c.

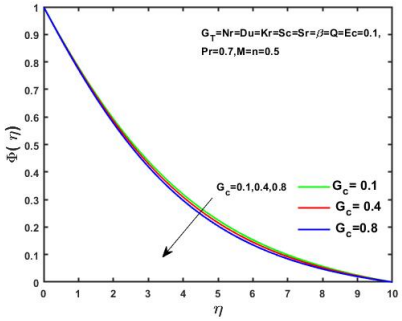

Figure 9: Concentration formulation of concentration Grashof number G_c.

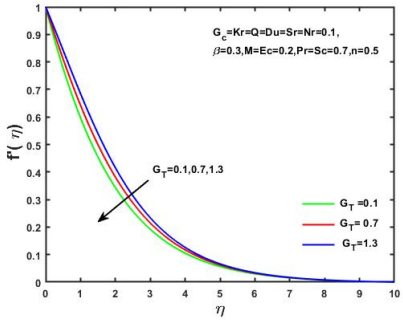

Figure 10: Velocity formulation of local thermal Grashof number G_T.

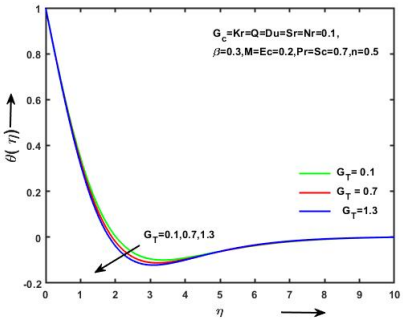

Figure 11: Temperature formulation of local thermal Grashof number G_T.

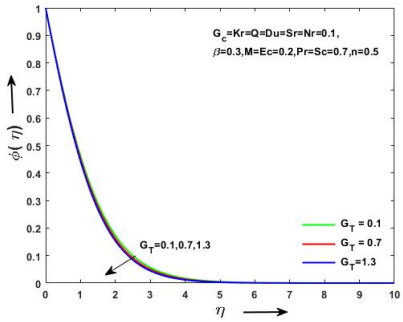

Figure 12: Concentration formulation of local thermal Grashof number G_T.

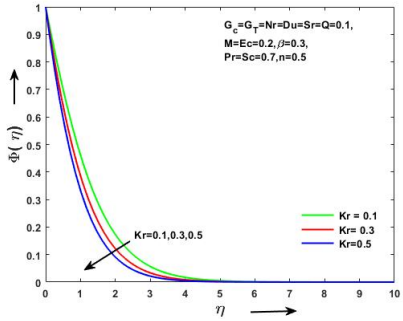

Figure 13: Concentration formulation of chemical reaction parameter Kr.

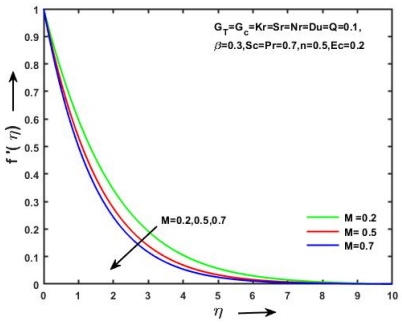

Figure 14: Velocity formulation of magnetic impact M.

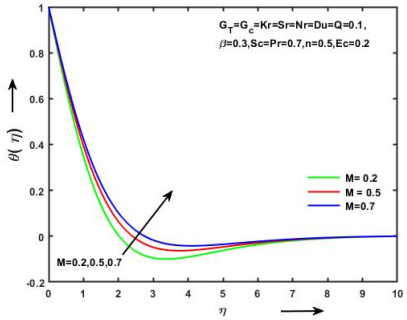

Figure 15: Temperature formulation of magnetic impact M.

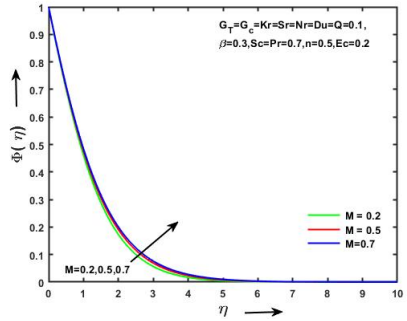

Figure 16: Volume fraction of magnetic impact M.

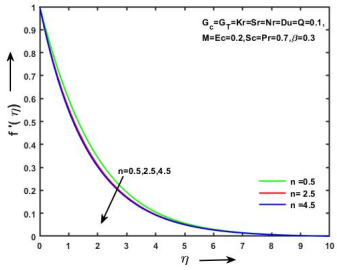

Figure 17: Motion formulation of the nonlinear parameter n.

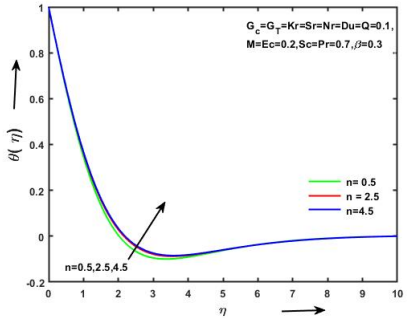

Figure 18: Temperature formulation of the nonlinear parameter n.

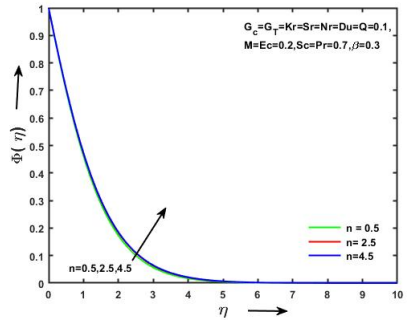

Figure 19: Concentration formulation of the nonlinear parameter n.

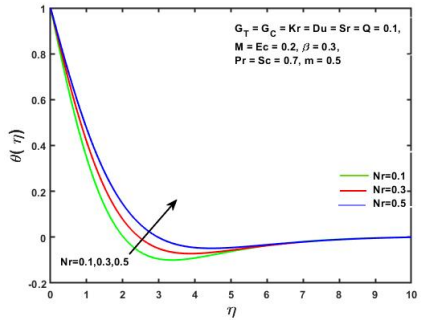

Figure 20: Temperature formulation of the Radiation parameter Nr.

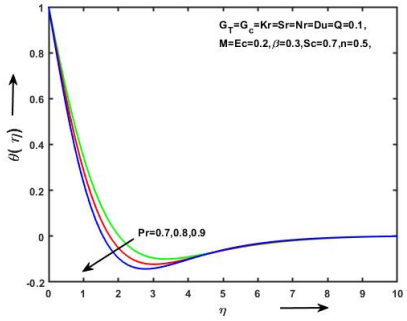

Figure 21: Temperature formulation of the Prandtl parameter Pr.

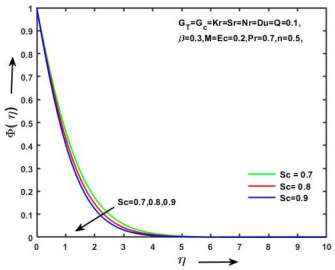

Figure 22: Concentration formulation of the Schmidt parameter Sc.

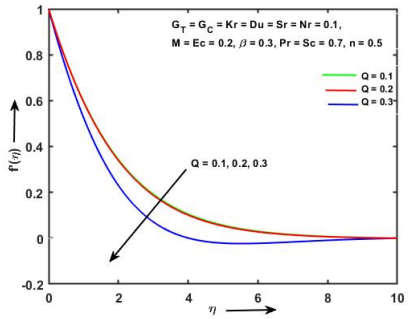

Figure 23: Motion formulations of Heat source sink Q.

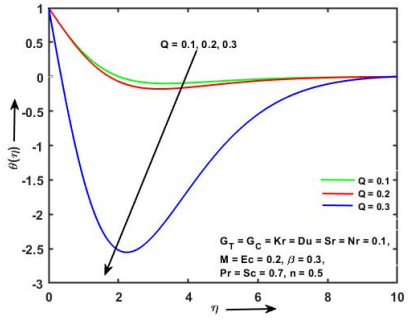

Figure 24: Temperature formulations of Heat source sink Q.

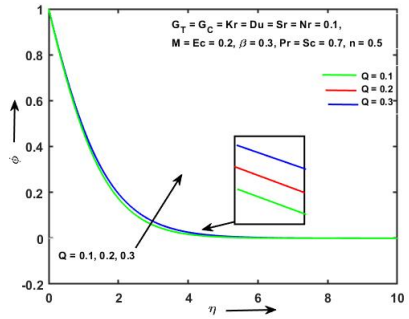

Figure 25: Concentration formulations of Heat source sink Q.

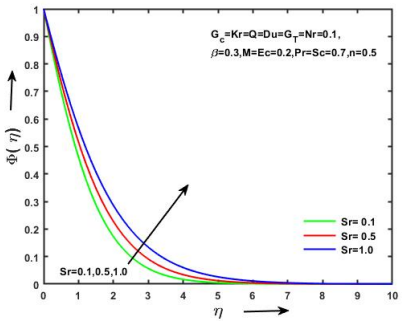

Figure 26: Concentration formulation of Soret effect Sr.

The impact of the thermal graph is displayed in Fig. 21 for various Prandtl number Pr quantities. Temperature distribution is shown to reduce for increasing in this analysis. Physically, Prandtl parameter Pr affects the thickness of the thermal boundary layer and momentum boundary layers. A larger Prandtl number denotes a thickness of the thermal boundary layer that is thinner, maintaining the boundary layer's uniform thermal distribution. The heating-boundary layer is subordinated to the magneto hydrodynamic boundary layer. Heat can dissipate more quickly in reduced Prandtl parameter fluids than in highest Prandtl parameter fluids according to their higher thermal conductivities. The impact of Schmidt parameter Sc on the dispensation of concentrations is shown in Fig.22. The volume fraction field reduces with rising Schmidt number Sc. Schmidt number, though it is constantly connected to velocity and mass diffusivities. Therefore, the fluid concentration diffusion is suppressed by rising values of Schmidt parameter Sc. In Figure 23, the motion profile reduces with the enhancing value of heat source or sink Q. Figure 24 shows how heating source or sink parameter Q affects temperature. The figure shows that as the heat sink's power rises, the non - dimensional temperature lowers, even as the heat source's power rises, the temperature rises. Therefore, as the heat sink parameter is raised, the thermal boundary layer reduces thickness, whereas the heat source effect causes it to rise. Also Fig.25 denotes the increasing concentration profile with the increasing value of heat source or sink Q. Figure 26 provided a visual representation of the consequences of thermal migration or Soret number (Sr). Sr represents the mass transfer rate between lowest to the highest solute concentrations and is essentially a ratio of temperature gradient to concentration. Figure 26 show that the concentration profile is exhibiting a rising behavior along with the rising value of Sr.

Table I: Impression of parameters of notice on skin friction, Nusselt parameter, and Sherwood parameter:

n	G_T	G_C	β	M	Pr	Ec	Sc	Q	Du	Sr	Nr	Kr	$Cf_x Re_x{}^{1/2}$	$-Nu_x Re_x{}^{-1/2}$	$-Sh_x Re_x{}^{-1/2}$
0.5													**-1.85657**	**0.65240**	**0.55783**
2.5	**0.1**	**0.1**	**0.3**	**0.2**	**0.7**	**0.2**	**0.7**	**0.1**	**0.1**	**0.1**	**0.1**	**0.1**	**-2.23135**	**0.65017**	**0.54858**
4.5													**-2.3244**	**0.64932**	**0.54636**
	0.1												**-1.85657**	**0.6524**	**0.55783**
0.5	**0.7**												**-1.59447**	**0.65546**	**0.56157**
	1.3												**-1.33728**	**0.65742**	**0.56520**
			0.3										**-1.85657**	**0.652401**	**0.557836**
	0.1		**0.7**										**-1.43724**	**0.535531**	**0.5621336**
			0.7										**-1.44060**	**0.482280**	**0.5611931**
				0.2									**-1.85657**	**0.652401**	**0.557836**
			0.3	**0.5**									**-2.33732**	**0.928422**	**0.508645**
				0.7									**-2.05587**	**0.571925**	**0.545825**

					0.7							**-1.85657**	**0.652401**	**0.55783**
				0.2	**0.8**							**-1.48080**	**0.727980**	**.561245**
					0.9							**-1.53126**	**0.79666**	**0.5589154**
						0.1						**-10.18979**	**2.044867**	**0.594878**
			0.02		**0.7**	**0.3**						**-26.32619**	**10.6900**	**0.507348**
						0.5						**-33.7957**	**18.38017**	**0.4583266**
							0.7					**-1.85657**	**0.652401**	**0.557836**
			0.3			**0.2**	**0.8**					**-2.01032**	**0.925019**	**0.558312**
							0.9					**-1.42483**	**0.648136**	**0.558312**
								0.1				**-1.85657**	**0.652401**	**0.557836**
							0.7	**0.2**				**-1.463515**	**0.626327**	**0.56106**
								0.3				**-1.63419**	**0.691826**	**0.551289**
									0.1			**-1.856577**	**0.652401**	**0.557836**
								0.1	**0.5**			**-1.9724632**	**0.809687**	**0.515012**
									1			**-1.222268**	**0.336784**	**0.573077**
										0.1		**-1.85657**	**0.652401**	**0.557836**
									0.1	**0.5**		**-1.419446**	**0.663674**	**0.494086**
										1		**-2.0097**	**0.948055**	**0.3811412**
											0.1	**-1.856577**	**0.652401**	**0.557836**
										0.1	**0.3**	**-1.34829**	**0.577117**	**0.56761**
											0.5	**-1.283884**	**0.51627**	**0.570809**
												0.1	**-1.856577**	**0.652401**	**0.557836**
											0.1	**0.2**	**-1.42427**	**0.6509020**	**0.64566**
												0.3	**-1.425672**	**0.645687**	**0.7180935**
		0.1											**-3.678953**	**0.75017**	**0.200603**
		0.4	**0.1**	**0.5**		**0.1**	**0.1**					**0.1**	**-3.2968876**	**0.7372915**	**0.20394816**
		0.8											**-2.803422**	**0.720553**	**0.208056**

Table II: validate the current values of various physical parameters to previouslyresults of Basha et al. Ref. [3] andVajraveluk. Ref. [21] respectively.

		Vajraveluk.Ref[21]		**Basha et al. Ref. [3]**		**current values**	
n	Pr	$f^{''}(0)$	$\theta'(0)$	$f^{''}(0)$	$\theta'(0)$	$f^{''}(0)$	$\theta'(0)$
1	**0.71**	**-1.0000**	**-0.4590**	**-1.00005468353233**	**-0.45908783553**	**-1.00001**	**-0.459033**
5	**0.71**	**-1.1945**	**-0.4394**	**-1.19449559110388**	**-0.4395495710690**	**-1.1945**	**-0.4394**
10	**0.71**	**-1.2348**	**-0.4357**	**-1.23488263663213**	**-0.4356401511209**	**-1.23488**	**-0.435641**
1	**7**	**-1.0000**	**-1.8953**	**-1.00005468353233**	**-1.8953100096284**	**-1.00001**	**-1.89541**
5	**7**	**-1.1945**	**-1.8610**	**-1.19449559110388**	**-1.8609911518168**	**-1.1945**	**-1.86159**
7	**7**	**-1.2348**	**-1.8541**	**-1.23488263663213**	**-1.8540100137230**	**-1.23488**	**-1.85464**

4 Conclusion:

From the current study we conclude that the mathematical outcomes for diverse physical quantities have been dissolved. The effects of the transfer of mass and heat including Soret and Dufour effects, heat absorption/ generation, Radiation parameter, chemical reaction, have been expressed for a non-linear stretchy surface in the rheology.This problem can be solved for future purpose if sheet is inclined at some angle. The boundary conditions and fluids can also be changed. The ending conclusion is

- An increasing value of Soret effect, grow the concentration of the fluid. And an increasing value of Heat source/ sink, also enhancing the concentration of the fluid

- Temperature profile is increased for an increasing value of Dufour effect
- Motion and thermal profiles of the fluid are decreased due to increased Heat source/sink
- Temperature profile of the fluid is increased when raised thermal radiation
- Motion and thermal profiles of the fluid are decreased due to enhanced Eckert number
- The decreasing skin-friction rate impression is seen for radiation parameters
- For the Soret effect, the diminishing Sherwood parameter impression is observed

References

[1] Ebrahem A Algehyne, Musaad S Aldhabani, Anwar Saeed, Abdullah Dawar, and Poom Kumam. Mixed convective flow of casson and oldroyd-b fluids through a stratified stretching sheet with nonlinear thermal radiation and chemical reaction. *Journal of Taibah University for Science*, 16(1):193–203, 2022.

[2] Sameh E Ahmed, MA Mansour, A Mahdy, and Shadia S Mohamed. Entropy generation due to double diffusive convective flow of casson fluids over nonlinearity stretching sheets with slip conditions. *Engineering Science and Technology, an International Journal*, 20(6):1553–1562, 2017.

[3] Mushtaq Ahmad, Muhammad Imran Asjad, and Jagdev Singh. Application of novel fractional derivative to heat and mass transfer analysis for the slippage flow of viscous fluid with single-wall carbon nanotube subject to newtonian heating. *Mathematical Methods in the Applied Sciences*, 2021.

[4] Hussain Basha, Naresh Kumar Nedunuri, Gudala Janardhana Reddy, and Sreenivasulu Ballem. Thermal analysis of buoyancy-motivated casson fluid flow with time-independent chemical reaction under lorentz forces. *Heat Transfer*, 50(7):7291–7320, 2021.

[5] Hussain Basha, Sreenivasulu Ballem, G Janardhana Reddy, Harish Holla, and Mikhail A Sheremet. Buoyancy-motivated dissipative free convection flow of walters-b fluid along a stretching sheet under the soret effect and lorentz force influence. *Heat Transfer*, 51(4):3512–3539, 2022.

[6] Subrata Das, Hiranmoy Mondal, Prabir Kumar Kundu, and Precious Sibanda. Spectral quasi-linearization method for casson fluid with homogeneous heterogeneous reaction in presence of nonlinear thermal radiation over an exponential stretching sheet. *Multidiscipline Modeling in Materials and Structures*, 2018.

[7] K Gangadhar, R Edukondala Nayak, and M Venkata Subba Rao. Buoyancy effect on mixed convection boundary layer flow of casson fluid over a non linear stretched sheet using the spectral relaxation method. *International Journal of Ambient Energy*, 43(1):1994–2002, 2022.

[8] Sami Ul Haq, Saeed Ullah Jan, Syed Inayat Ali Shah, Ilyas Khan, and Jagdev Singh. Heat and mass transfer of fractional second grade fluid with slippage and ramped wall temperature using caputo-fabrizio fractional derivative approach. *AIMS Mathematics*, 5(4):3056–3088, 2020.

[9] Abid Hussanan, Mohd Zuki Salleh, Hamzeh Taha Alkasasbeh, and Ilyas Khan. Mhd flow and heat transfer in a casson fluid over a nonlinearly stretching sheet with newtonian heating. *Heat transfer research*, 49(12), 2018.

[10] SM Ibrahim, G Lorenzini, P Vijaya Kumar, and CSK Raju. Influence of chemical reaction and heat source on dissipative mhd mixed convection flow of a casson nanofluid over a nonlinear permeable stretching sheet. *International Journal of Heat and Mass Transfer*, 111:346–355, 2017.

[11] Sweta Matta, Appidi L BalaSiddaluMalga, and P Pramod Kumar. Radiation and chemical reaction effects on unsteady mhd free convention mass transfer fluid flow in a porous plate. *Indian Journal of Science and Technology*, 14(8):707–717, 2021.

[12] Ruchika Mehta, Ravindra Kumar, Himanshu Rathore, and Jagdev Singh. Joule heating effect on radiating mhd mixed convection stagnation point flow along vertical stretching sheet embedded in a permeable medium and heat generation/absorption. *Heat Transfer*, 51(8):7369–7386, 2022.

[13] Monica Medikare, Sucharitha Joga, Kishore Kumar Chidem, et al. Mhd stagnation point flow of a casson fluid over a nonlinearly stretching sheet with viscous dissipation. *American Journal of Computational Mathematics*, 6(01):37, 2016.

[14] M Mustafa and Junaid Ahmad Khan. Model for flow of casson nanofluid past a non-linearly stretching sheet considering magnetic field effects. *AIP advances*, 5(7):077148, 2015.

[15] Swati Mukhopadhyay. Casson fluid flow and heat transfer over a nonlinearly stretching surface. *Chinese Physics B*, 22(7):074701, 2013.

[16] NB Naduvinamani and Usha Shankar. Thermal-diffusion and diffusion-thermo effects on squeezing flow of unsteady magneto-hydrodynamic casson fluid between two parallel plates with thermal radiation. *Sādhanā*, 44(8):1–16, 2019.

[17] Satyaban Panigrahi, Motahar Reza, and Akshya Kumar Mishra. Mixed convective flow of a powell-eyring fluid over a non-linear stretching surface with thermal diffusion and diffusion thermo. *Procedia Engineering*, 127:645–651, 2015.

[18] P Bala Anki Reddy. Magnetohydrodynamic flow of a casson fluid over an exponentially inclined permeable stretching surface with thermal radiation and chemical reaction. *Ain Shams Engineering Journal*, 7(2):593–602, 2016.

[19] Jagdev Singh, Devendra Kumar, Dumitru Baleanu, et al. A hybrid analytical algorithm for thin film flow problem occurring in non-newtonian fluid mechanics. *Ain Shams Engineering Journal*, 12(2):2297–2302, 2021.

[20] Jagdev Singh, Devendra Kumar, and Sunil Kumar. An efficient computational method for local fractional transport equation occurring in fractal porous media. *Computational and Applied Mathematics*, 39(3):1–10, 2020.

[21] Chenna Sumalatha, Shankar Bandari, et al. Effects of radiations and heat source/sink on a casson fluid flow over nonlinear stretching sheet. *World Journal of Mechanics*, 5(12):257, 2015.

[22] Gandluru Sreedevi, DRV Rao, Oluwole Daniel Makinde, and G Reddy. Soret and dufour effects on mhd flow with heat and mass transfer past a permeable stretching sheet in presence of thermal radiation. 2017.

[23] Shyam Sunder Tak, Rajeev Mathur, Rohit Kumar Gehlot, and Aiyub Khan. Mhd free convection-radiation interaction along a vertical surface embedded in darcian porous medium in presence of soret and dufour's effects. *Thermal Science*, 14(1):137–145, 2010.

[24] Imran Ullah, Sharidan Shafie, and Ilyas Khan. Effects of slip condition and newtonian heating on mhd flow of casson fluid over a nonlinearly stretching sheet saturated in a porous medium. *Journal of King Saud University-Science*, 29(2):250–259, 2017.

[25] Imran Ullah, Ilyas Khan, and Sharidan Shafie. Soret and dufour effects on unsteady mixed convection slip flow of casson fluid over a nonlinearly stretching sheet with convective boundary condition. *Scientific Reports*, 7(1):1–19, 2017.

[26] K Vajravelu. Viscous flow over a nonlinearly stretching sheet. *Applied mathematics and computation*, 124(3):281–288, 2001.